Adiabatic, Shock, and Plastic Work Heating of Solids and the Cylinder Test

E. L. Ruden and G. F. Kiuttu

May 2000

Final Report

20010305 092

AIR FORCE RESEARCH LABORATORY
Directed Energy Directorate
3550 Aberdeen Ave SE
AIR FORCE MATERIEL COMMAND
KIRTLAND AIR FORCE BASE, NM 87117-5776

This report has been reviewed by the Public Affairs Office and is releasable to the National Technical Information Service (NTIS). At NTIS, it will be available to the general public, including foreign nationals.

If you change your address, wish to be removed from this mailing list, or your organization no longer employs the addressee, please notify AFRL/DEHP, 3550 Aberdeen Ave SE, Kirtland AFB, NM 87117-5776.

Do not return copies of this report unless contractual obligations or notice on a specific document requires its return.

This report has been approved for publication.

E. L. RUDEN, DR-II
Project Manager

FOR THE COMMANDER

COURTNEY D. HOLMBERG, Major, USAF   R. EARL GOOD, SES
Chief, High Power Microwave Division   Director, Directed Energy

REPORT DOCUMENTATION PAGE

1. AGENCY USE ONLY (Leave blank)	2. REPORT DATE May 2000	3. REPORT TYPE AND DATES COVERED Final Report, Dec 1999 – May 2000

4. TITLE AND SUBTITLE
Adiabatic, Shock, and Plastic Work Heating of Solids and the Cylinder Test

5. FUNDING NUMBERS

PE: 61102F
PR: 2301
TA: ER
WU: 06

6. AUTHOR(S)
E. L. Ruden and G. F. Kiuttu

7. PERFORMING ORGANIZATION NAME(S) AND ADDRESS(ES)

Air Force Research Laboratory
AFRL/DEHP
3550 Aberdeen Ave SE
Kirtland AFB, NM 87117-5776

8. PERFORMING ORGANIZATION REPORT NUMBER
AFRL-DE-TR-2000-1100

9. SPONSORING / MONITORING AGENCY NAME(S) AND ADDRESS(ES)

10. SPONSORING / MONITORING AGENCY REPORT NUMBER

11. SUPPLEMENTARY NOTES

12a. DISTRIBUTION / AVAILABILITY STATEMENT
Approved for Public Release; Distribution is Unlimited.

12b. DISTRIBUTION CODE

13. ABSTRACT *(Maximum 200 Words)*
Solids subjected to high pressures, shocks, and/or deformation experience an increase in internal energy density and temperature due to adiabatic compression, shock heating, and plastic work heating, respectively. Analytic approximations are derived here for the internal energy and temperature changes that result from these processes based on the analytic constitutive model and Grüneisen equation of state of D. Steinberg. Although of general use, the utility of the expressions is demonstrated by the detailed example of a cylindrical metal tube filled with high explosives and detonated on axis at one end. This geometry is often used to determine the detonation properties of high explosives, where it is known as the "cylinder test". The geometry is also of special interest for use as the armature of cylindrical magnetic flux compression pulsed current generators. The results are favorably compared with two dimension numerical simulations of the process using Lawrence Livermore National Laboratory's shock-hydro computer code GALE using the same model for the metal.

14. SUBJECT TERMS
Adiabatic shock plastic work heating of solids cylinder test

15. NUMBER OF PAGES
28

16. PRICE CODE

17. SECURITY CLASSIFICATION OF REPORT UNCLASSIFIED	18. SECURITY CLASSIFICATION OF THIS PAGE UNCLASSIFIED	19. SECURITY CLASSIFICATION OF ABSTRACT UNCLASSIFIED	20. LIMITATION OF ABSTRACT UNLIMITED

Table Of Contents

Table of Charts and Figures

Adiabatic, Shock, and Plastic Work Heating of Solids and the Cylinder Test

E. L. Ruden and G. F. Kiuttu

Air Force Research Laboratory

AFRL/DEHP

3550 Aberdeen Ave. SE

Kirtland AFB, NM 87117-5776

email: ruden@plk.af.mil

(May 11, 2000)

Abstract

Solids subjected to high pressures, shocks, and/or deformation experience an increase in internal energy density and temperature due to adiabatic compression, shock heating, and plastic work heating, respectively. Analytic approximations are derived here for the internal energy and temperature changes that result from these processes based on the analytic constitutive model and Grüneisen equation of state of D. Steinberg. Although of general use, the utility of the expressions is demonstrated by the detailed example of a cylindrical metal tube filled with high explosives, and detonated on axis at one end. This geometry is often used to determine the detonation properties of high explosives, where it is known as the "cylinder test". The geometry is also of special interest for use as the armature of cylindrical magnetic flux compression pulsed current generators. The results are favorably compared with two dimension numerical simulations of the process using Lawrence Livermore National Laboratory's shock-hydro computer code CALE using the same model for the metal.

I. INTRODUCTION

This paper was originally motivated by a need to better understand the thermodynamic evolution of explosively expanded metal tubes. AFRL's Directed Energy Directorate (DE) is developing explosive axial magnetic flux compression [pulsed current] generators [1] (FCG's) suitable as the primary energy source for expendable devices requiring very high electrical pulsed power. These generators use a cylindrical metal armature filled with high explosive and detonated on axis at one end. This geometry is independently known as the "cylinder test" in explosives research, being well suited for the analysis of the properties of explosive products [22]. In the generator application, axial magnetic flux trapped between the expanding armature and a surrounding helically wound stator is compressed, generating high

2

current. The shock to, and plastic expansion of the armature results in an increase in the armature's temperature, leading to increased electrical resistivity and possible melting. If melting occurs, further flux compression is impaired by a greatly enhanced Rayleigh-Taylor instability. Even before melting, the expansion process itself can become unstable, with the armature fragmenting by plastic instability. These processes result in decreased performance, and more detailed modeling of them is necessary. The principle tool used for modeling the pulsed power circuit is CAGEN [2], which couples a lumped circuit to a zero dimensional simulation of the generator for which the armature is characterized by its outer radius as a function of axial position and time $R(z,t)$. One application of results presented here is to improve the electrical resistivity treatment of the armature model in programs like CAGEN. Given additional simplifying assumptions, energy and temperature estimates are rendered in purely analytic form. In the process, analytic solutions to energy and temperature changes due to basic mechanical processes are derived based on Steinberg's form [3] of the Grüneisen equation of state [4] and the Steinberg-Cochran-Guinan constitutive relations for material strength [5], hereafter referred to as the "Steinberg model". These general solutions are the primary emphasis of this paper because of their wider potential interest, with the cylinder test application presented thereafter as a detailed example their utility.

The Steinberg model is a popular dynamic model of solids, especially metals, which undergo high rates of strain and compression ($\gtrsim 10^5$ s^{-1}). Many materials have been characterized for it [3], and it is used in several hydrodynamic and magnetohydrodynamic computer codes [6] [7] [8] [9] [10] [11]. Despite the model's analytic form, though, its potential for deriving approximate analytic solutions has not been well exploited. The more general expressions presented should prove to be useful tools for studying a wide variety of dynamically deforming geometries. The symbolic form of the expressions should make various dependences on variables more apparent and parameter space surveys easier to accomplish than with codes alone. Follow-up with computer modeling of promising configurations thereby identified may then be pursued more productively.

3

Section II reviews adiabatic compression in the Steinberg model and provides useful approximations for internal energy per unit mass E and temperature T along the adiabat. These expressions are needed to calculate T as a function of compression and E more generally. Section III derives E and T approximations that result from planar shocks traversing a solid with standard initial conditions. Section IV derives an expression for the change in E as a function of the equivalent deviatoric strain ϵ resulting from plastic deformation. This expression is particularly useful because it takes into account the important effects work hardening and thermal softening in the Steinberg model, although elasticity, compressibility, and the pressure dependence of the yield strength are neglected. Section V presents a detailed example of how the derived expressions may be used for explosively expanded cylinders. Section VI presents results of two dimensional numerical simulations of this cylinder test for comparison with the analytic expressions to gauge how well the analytic approximations represent the Steinberg model. Discussion of the empirical validity of the model itself is covered in the supplied references and is considered beyond the scope of this paper.

One shortcoming of the approximations presented for shock heating and plastic work is that they assume both processes do not occur simultaneously. A more unified thermomechanical treatment is required, in particular, where shocks are strongly nonplanar, such as in impact cratering. Fortunately, there are many other cases where one process dominates the other or they occur on different time scales. The cylinder test presented is an example of the latter. Thermal conductivity is neglected throughout due to the short time scales of the processes involved.

II. TEMPERATURE AND ADIABATIC HEATING

The Steinberg model's relationship between pressure P, density ρ, and internal energy per unit mass relative to that at standard conditions ($P = 0$, temperature $T = T_R = 300K$) E is [5],

$$P(\mu, E) = \begin{cases} \dfrac{\rho_0 C_0^2 \mu \left[1 + \left(1 - \frac{\gamma_0}{2}\right)\mu - \frac{b}{2}\mu^2\right]}{\left[1 - (S_1 - 1)\mu - S_2 \frac{\mu^2}{\mu + 1} - S_3 \frac{\mu^3}{(\mu + 1)^2}\right]^2} + (\gamma_0 + b\mu)\,\rho_0 E & \text{if } \mu > 0 \\[4mm] \rho_0 C_0^2 \mu + \rho_0 \gamma_0 E & \text{if } \mu \le 0 \end{cases} \tag{1}$$

Here, $\mu = \rho/\rho_0 - 1$ and C_0 (sound speed), ρ_0 (standard density), γ_0, b, S_1, S_2, and S_3 are available phenomenological parameters [3] described more fully in the references.

To find an expression for T, we start with $T = (E - E_c)/C$ for fixed μ, where C is specific heat (assumed constant in the Steinberg model) and $E_c = E$ at compression μ and $T = 0$ [5]. Subtracting both sides of this equation, solved for the special case of the adiabat from standard conditions were $T = T_0(\mu)$ and $E = E_0(\mu)$, from the respective sides of the general case results in,

$$T(E, \mu) = T_0(\mu) + \frac{E - E_0(\mu)}{C} \tag{2}$$

$T_0(\mu)$ may be found from the adiabatic relationship [12],

$$T_0 = T_R \exp\left[-\int_{V_0}^{V} \frac{\gamma(V')}{V'} dV'\right] \qquad \gamma(V) = V\left(\frac{\partial P}{\partial \mathcal{E}}\right)_V \tag{3}$$

where V is a sample volume (with V_0 its standard conditions value), $\mathcal{E}$ is internal energy, and γ is the Grüneisen ratio [12] [3]. Changing variables via $V = V_0/(\mu + 1)$ and $\mathcal{E} = \rho_0 V_0 E$, using Eq. 1 for P, and integrating,

$$T_0(\mu) = \begin{cases} T_R (\mu + 1)^b \exp\left(\frac{(\gamma_0 - b)\mu}{\mu + 1}\right) & \text{if } \mu > 0 \\[3mm] T_R \exp\left(\frac{\gamma_0 \mu}{\mu + 1}\right) & \text{if } \mu \le 0 \end{cases} \qquad \gamma(\mu) = \frac{\gamma_0 + b\mu}{\mu + 1} \tag{4}$$

This expression may be recognized as a generalization the Steinberg model's melting temperature [3], which is assumed to follow the adiabat.

$E_0(\mu)$, meanwhile, may be found from Eq. 1 since $d\mathcal{E} = -PdV$ along an adiabat. This results in the following differential equation and its solution [13],

$$\frac{dE}{d\mu} = \frac{P(\mu, E)}{\rho_0(\mu + 1)^2} \qquad E_0(\mu) = \frac{T_0(\mu)}{\rho_0} \int_0^{\mu} \frac{P(\mu', 0)}{(\mu' + 1)^2 T_0(\mu')} d\mu' \tag{5}$$

This expression may be approximated to within 2% in the specified ranges by,

$$
E_0(\mu) \approx \begin{cases} \frac{C_0^2 T_0(\mu)}{T_R} \sum_{i=2}^{4} a_i \mu^i & \text{if} \quad 0 < \mu < 0.35 \\[2mm] \frac{C_0^2 T_0(\mu)}{T_R} \sum_{i=2}^{5} b_i \mu^i & \text{if} \quad -0.20 < \mu \le 0 \end{cases}
$$

$$
a_2 = \tfrac{1}{2} \qquad\qquad a_3 = \tfrac{1}{6} \left(4S_1 - 6 - 3\gamma_0 \right)
$$

$$
a_4 = 800 \exp\left(\tfrac{(b-\gamma_0)}{5} \right) \left(\tfrac{4}{5} \right)^b \frac{40 - 4\gamma_0 - b}{(25 S_1 + 5 S_2 + S_3 - 125)^2} - \left(2S_1 - 3 - \tfrac{3}{2}\gamma_0 \right) - 4 \tag{6}
$$

$$
b_2 = \tfrac{1}{2} \qquad b_3 = -\tfrac{1}{3}\left(2 + \gamma_0 \right) \qquad b_4 = \tfrac{1}{8}\left(6 + 6\gamma_0 + \gamma_0^2 \right)
$$

$$
b_5 = \tfrac{4}{245} \left(-8192 \exp\left(\tfrac{\gamma_0}{7} \right) + 8134 + 1078\gamma_0 + 49\gamma_0^2 \right)
$$

The coefficients are determined by Taylor expansion of the integrand of Eqs. 5, except for a_4 and b_5. For greater accuracy, the latter are chosen to make the integrand error zero at $\dot{\mu}' = -\tfrac{1}{8}$ and $\tfrac{1}{4}$.

III. SHOCK HEATING

If we assume the external pressure rises instantaneously from 0 to a constant P_1 upon the arrival of a planar shock wave through an initially stationary solid with standard conditions, the shocked material properties can be described by the Hugoniot relations [14], expressible as,

$$
v_s^2 = \frac{(\mu_1 + 1) P_1}{\mu_1 \rho_0} \qquad K_1 \equiv \frac{v_1^2}{2} = E_1 = \frac{\mu_1 P_1}{2\rho_0 (\mu_1 + 1)} \qquad \mu_1 = \frac{\rho_1}{\rho_0} - 1 \tag{7}
$$

ρ_1, v_1, P_1, E_1, and K_1 are density, velocity, P, E, and kinetic energy per unit mass behind the shock, respectively, and v_s is shock speed. Substituting E_1 in Eqs. 7 into Eq. 1, with $P = P_1$, and solving for P_1 gives us our Hugoniot function,

$$
P_1 = \frac{\rho_0 C_0^2 \mu_1 (\mu_1 + 1)}{\left[1 - (S_1 - 1)\mu_1 - S_2 \frac{\mu_1^2}{\mu_1 + 1} - S_3 \frac{\mu_1^3}{(\mu_1 + 1)^2} \right]^2} \tag{8}
$$

For modest compressions, we may neglect the S_2 and S_3 terms [15]. Eq. 8, then, reduces to a quadratic in μ_1 with (meaningful) solution,

$$
\mu_1 = \frac{\sqrt{4\Pi S_1 + 1} - 2\Pi(S_1 - 1) - 1}{2 - 2\Pi(S_1 - 1)^2} \qquad\qquad \Pi = \frac{P_1}{\rho_0 C_0^2} \tag{9}
$$

6

Plugging this into (Eqs. 7) gives,

$$v_s^2 = \frac{\Pi C_0^2}{\alpha_1} \qquad\qquad K_1 \equiv \frac{v_1^2}{2} = E_1 = \frac{\alpha_1 \Pi C_0^2}{2} \tag{10}$$

$$\alpha_1 = \frac{\mu_1}{\mu_1 + 1} = \frac{\sqrt{4\Pi S_1 + 1} - 2\Pi(S_1 - 1) - 1}{\sqrt{4\Pi S_1 + 1} - 2\Pi S_1(S_1 - 1) + 1} \tag{11}$$

The temperature behind the shock is, from Eq. 2,

$$T_1 = T(E_1, \mu_1) \tag{12}$$

One important application to the solutions above is the case of a explosive detonation wave which interacts with a plate or shell. In this case, the initial shock compression unloads at the surface opposite the explosive, sending an continuous adiabatic rarefaction wave inward. Some energy is transmitted back into the explosive products, and some reflects as a second outward shock. $E_1 - E_0(\mu_1)$ is the irreversible contribution to the energy behind the initial shock and is, therefore, a *lower bound* on the final energy E_s after the explosive products and waves dissipate, and pressure falls off. Before this, though, secondary shocks and rarefactions continue to increase heat and smooth the pressure profile, respectively. An *upper bound* on E_s is E_1 itself, so we have,

$$E_1 - E_0(\mu_1) \leq E_s \leq E_1 \tag{13}$$

To find the temperature corresponding to $E = E_s$ after pressure fall off, we solve to Eq. 1 for $\mu = -\gamma_0 E/C_0^2$ (negative due to thermal expansion) at $P = 0$ and plug into Eq. 2,

$$T = T(E, -\gamma_0 E/C_0^2) \qquad\qquad (P = 0) \tag{14}$$

IV. PLASTIC WORK HEATING

The contribution to E from plastic work heating E_p as a function of E's initial value E_s and equivalent plastic strain ϵ may be derived in closed form for the Steinberg model,

7

provided we neglect compressibility, elasticity, the pressure dependence of the uniaxial yield strength Y, and other active heat sources. The (usually more important) effects of work hardening and thermal softening of the material are retained, however. Though E_s is of arbitrary value in this section, we use the same symbol that was used for shock heating in the previous section to suggest one potential origin.

Neglecting elasticity, the Levy-Mises (L-M) relation for rigid plastic flow is [16],

$$\mathbf{D} \equiv \frac{1}{2}(\nabla \mathbf{v} + \nabla \mathbf{v^T}) = \frac{3}{2}\frac{d\epsilon}{dt}\frac{\mathbf{S}}{Y} \qquad \epsilon \equiv \frac{2}{\sqrt{6}} \int \sqrt{\mathbf{D} \cdot \mathbf{D}} dt \qquad (15)$$

where $\mathbf{D}$ and $\mathbf{S}$ are the deviatoric strain rate and stress tensors, respectively. The Steinberg model's strain rate independent material strength equation [5] is,

$$Y = \left[1 + \frac{AP}{(1+\mu)^{\frac{1}{3}}} - B(T - T_R)\right] \times \begin{cases} Y_0\left[1 + \beta(\epsilon + \epsilon_i)\right]^n & \text{if } \epsilon < \epsilon_c \\ Y_{\max} & \text{if } \epsilon \geq \epsilon_c \end{cases} \qquad (16)$$

where A, B, β, n, $Y_{\max}$, and Y_0, and ϵ_i are phenomenological parameters tabulated for several materials [3], and,

$$\epsilon_c = \frac{(Y_{\max}/Y_0)^{1/n} - 1}{\beta} - \epsilon_i \qquad (17)$$

We neglect the P dependent term in Eq. 16 and use, assuming incompressibility, $(T - T_R) = E/C$, from Eq. 2. Given these assumptions, the plastic work rate [16] per unit mass is, using Eqs. 15 and Eq. 16,

$$\frac{dE_p}{dt} \equiv \frac{\mathbf{S} \cdot \mathbf{D}}{\rho} = \frac{Y}{\rho_0}\frac{d\epsilon}{dt} = \frac{1 - \frac{B}{C}E}{\rho_0}\frac{d\epsilon}{dt} \times \begin{cases} Y_0\left[1 + \beta(\epsilon + \epsilon_i)\right]^n \\ Y_{\max} \end{cases} \qquad (18)$$

where ρ_0 is the standard mass density of the material (assumed constant). Here and henceforth, the upper and lower expressions are for $\epsilon < \epsilon_c$ and $\epsilon \geq \epsilon_c$, respectively, unless otherwise specified. Assuming further that there is no other active heat source, then $E = E_p + E_s$, and Eq. 18 is reducible to a differential equation in E_p with reference to ϵ with solution,

$$E_p = \left(\frac{C}{B} - E_s\right) - \left(\frac{C}{B} - E_s\right) \times$$

$$\begin{cases} \exp\left[-\frac{BY_0}{C\rho_0\beta(n+1)}\left([1+\beta(\epsilon+\epsilon_i)]^{n+1}-[1+\beta\epsilon_i]^{n+1}\right)\right] \\ \exp\left[-\frac{BY_0}{C\rho_0\beta(n+1)}\left([1+\beta(\epsilon_c+\epsilon_i)]^{n+1}-[1+\beta\epsilon_i]^{n+1}\right)-\frac{BY_{\max}}{C\rho_0}(\epsilon-\epsilon_c)\right] \end{cases} \tag{19}$$

Note, if thermal softening is neglected, one must take the limit of $B \to 0$, or (better yet) resolve Eq. 18 with $B = 0$,

$$\lim_{B\to 0} E_p = \begin{cases} \frac{Y_0}{\rho_0\beta(n+1)}\left([1+\beta(\epsilon+\epsilon_i)]^{n+1}-[1+\beta\epsilon_i]^{n+1}\right) \\ \frac{Y_0}{\rho_0\beta(n+1)}\left([1+\beta(\epsilon_c+\epsilon_i)]^{n+1}-[1+\beta\epsilon_i]^{n+1}\right)+\frac{Y_{\max}}{\rho_0}(\epsilon-\epsilon_c) \end{cases} \tag{20}$$

$E = E_s + E_p$ may now be used in Eq. 14 to determine the temperature.

V. EXAMPLE - EXPLOSIVELY EXPANDED TUBE

A. Geometry

We consider the example of a long (compared to its diameter) cylindrical tube of ductile metal loaded with high explosive and detonated on axis at one end. Upper and lower bounds on the shock heating of the tube, an estimate of the subsequent plastic work heating as the tube wall flares outward into a cone, and (as a caveat) the critical radius for the onset of plastic instability are derived. Much analytic theory [17] [18] [19] [20], computational modeling [21] [22], and experimental results [18] [23] [22] have been published on the this geometry, with details of the detonation wave and explosive products properties and interaction particularly well covered. Emphasis here will be placed instead on the thermal response of the tube material itself. Fortunately, for the simplest approximations presented, effects of the explosive products on shock heating and plastic work as a function of the expanding radius of the cylinder can be parameterized by the pressure P_1 behind the initial shock that traverses the tube wall after the detonation wave passes and the ratio V_r/D, where V_r is the radial expansion speed of the tube after it has expanded by a significant amount relative to the initial radius and D is the detonation speed. Existing models to estimate these two parameters are referenced.

B. Initial shock heating

The detonation wave in the subject case is primarily transverse to the inner cylinder wall. P_1 may be estimated by an available model [24] which assumes the explosive products can be described by Prandtl-Meyer flow around a sharp corner [25] with a self-consistently determined angle created by the compression of the tube wall due to the first shock. A necessary condition for this is that D be larger than the shock speed in the solid. This is the case for most high explosives on metals other that Be . An ideal gas with constant gamma adiabatic law for the products with the Chapman-Jouget (C-J) values for the initial pressure P_j, density ρ_j, and particle speed v_j behind the shock are assumed [26] [27],

$$P = P_i \left(\frac{\rho}{\rho_j}\right)^{\gamma_j} \qquad P_j = \frac{\rho_x D^2}{\gamma_j + 1} \qquad \rho_j = \frac{\gamma_j + 1}{\gamma_j} \rho_x \qquad v_j = \frac{D}{\gamma_j + 1} \qquad (21)$$

Here, ρ_x is the explosive's initial density, and γ_j is a phenomenological parameter. Higher order shock terms S_2 and S_3 in the metal's EOS are neglected, as was done in Section III.

To simplify Neal's solution to P_1, we note the integral required to obtain the plate surface deflection angle α, based on the explosive product response (Neal's Eq. 6), has solution,

$$\alpha = \sqrt{\frac{\gamma_j + 1}{\gamma_j - 1}} \arccos \eta - \frac{1}{2} \left(\arccos \frac{\sqrt{\gamma_j + 1}\eta + \sqrt{2}}{\sqrt{\gamma_j + 1} + \sqrt{2}\eta} + \arccos \frac{\sqrt{\gamma_j + 1}\eta - \sqrt{2}}{\sqrt{\gamma_j + 1} - \sqrt{2}\eta} \right) \qquad (22)$$

where η is defined below. η may also be expressed in terms of the angle θ between the metal shock front and the z-axis with the help of the equations which describe the metal's self-consistent response to P_1 (Neal's Eq. 10 and Eq. 12),

$$\eta \equiv \left(\frac{P_1}{P_j}\right)^{\frac{\gamma_j - 1}{2\gamma_j}} = \left(\frac{\rho_0 D^2}{P_j} \left(1 - \frac{D(S_1 - 1)\sin\theta + C_0}{DS_1 \sin\theta}\right) \sin^2\theta\right)^{\frac{\gamma_j - 1}{2\gamma_j}} \qquad (23)$$

Meanwhile, Neal's Eq. 12 solved for α, is,

$$\alpha = \theta - \arctan\left(\frac{D(S_1 - 1)\sin\theta + C_0}{DS_1 \cos\theta}\right) \qquad (24)$$

Intersecting this with Eq. 22, using the second expression in Eq. 23 for η, gives θ and therefore, from Eq. 23, P_1. An good starting point for Newton's method to find this intersection is the average of,

$$\theta_{\min} = \arcsin\left(\frac{C_0}{D}\right) \quad \text{and} \quad \theta_{\max} = \arcsin\frac{\rho_0 C_0 + \sqrt{\rho_0^2 C_0^2 + 4\rho_0 P_j S_1}}{2\rho_0 D} \tag{25}$$

$\theta_{\min}$ corresponds to the acoustic limit for metal shock speed, and $\theta_{\max}$ corresponds to $\eta = 1$ ($P_1 = P_j$) in Eq. 23. There is no real and meaningful solution to Eq. 22 outside this range. Generally speaking, one obtains values of P_1 for the metal shock roughly half that obtained from the more commonly treated case of the interaction of a detonation wave normally incident to the interface [28].

After obtaining an estimate of P_1, E_1 and bounds on E_s may be found from Eq. 10 and Eq. 13, respectively.

C. Subsequent plastic deformation

Given an axisymmetric thin walled shell of radius $R = R(z,t)$ expanding at radial velocity $V = V(z,t)$, and zero axial velocity, nonzero components of $\mathbf{D}$ and ϵ are, from Eqs. 15,

$$(D_{rr}, D_{\theta\theta}, D_{zz}) = (-1, 1, 0)\frac{V}{R} \qquad D_{rz} = D_{zr} = \frac{1}{2}\frac{\partial V}{\partial z} \tag{26}$$

$$\epsilon = \frac{2}{\sqrt{3}}\int\left[\left(\frac{V}{R}\right)^2 + \left(\frac{1}{2}\frac{\partial V}{\partial z}\right)^2\right]^{\frac{1}{2}} dt \tag{27}$$

In a thin shell model where $R(z,t)$ is independently determined and there are no other active heat sources, Eq. 27 may be plugged into Eq. 19 directly to determine $E_p(z,t)$. On the other hand, if other active sources of heat *are* present, differentiating Eq. 27 w.r.t. t and plugging into Eq. 18 gives us the more general expression for the plastic work contribution to the heating rate,

$$\frac{dE_p}{dt} = \frac{2\left(1 - \frac{B}{C}E\right)}{\sqrt{3}\rho_0}\left[\left(\frac{V}{R}\right)^2 + \left(\frac{1}{2}\frac{\partial V}{\partial z}\right)^2\right]^{\frac{1}{2}} \times \begin{cases} Y_0\left[1 + \beta\left(\epsilon + \epsilon_i\right)\right]^n \\ Y_{\max} \end{cases} \tag{28}$$

To simplify things further, a reasonable estimate of the plastic heating may be made by using the following approximations for V and, from Eq. 27, ϵ,

11

$$V = V_r \Theta(Dt - z) \qquad \epsilon = \frac{2}{\sqrt{3}} \ln \frac{R}{R_0} + \frac{V_r}{\sqrt{3}D} \text{ for } t > \frac{z}{D} \qquad (29)$$

Here, V_r and D are the radial expansion velocity and the axial explosive detonation velocity, respectively, and both are assumed constant. $\Theta(z)$ is the Step Function. In other words, we assume the armature is stationary until a purely axial shock front passes, at which time the armature is instantaneously accelerated to radial velocity V_r, flaring out into a conical shape. The simplest approximation for V_r, meanwhile, is provided by the Gurney Equation [17] [20],

$$V_r = \sqrt{2E_x} \left(\frac{M}{M_x} + \frac{1}{2} \right)^{-\frac{1}{2}} \qquad (30)$$

where M is the total cylinder mass, and M_x and E_x are the total explosive mass and phenomenological "Gurney energy" (liberated chemical energy per unit mass), respectively. Given V_r and D, ϵ from Eq. 29 may be substituted directly into Eq. 19 to determine E_p. One may then add E_p to the bounds on E_s and use Eq. 14 to bound the temperature due the combined effects of shock and plastic work heating.

In the above, azimuthal symmetry is assumed. It is worth noting, however, that expansion beyond a critical point is unstable, and after a period of subsequent instability growth, the liner will fail. A band of ductile material being stretched will undergo plastic instability when the relative increase in the yield strength dY/Y due to work hardening over a time interval dt falls below the relative decrease in the band's cross sectional area dA/A. In the incompressible limit, this occurs when [29] $Y = dY/d\epsilon$. From Eq. 16, neglecting thermal softening, this condition is met when ϵ reaches the following value, which corresponds to the given radius, based on Eq. 29,

$$\epsilon_p = \begin{cases} n - \frac{1}{\beta} - \epsilon_i & \text{if } n - \frac{1}{\beta} - \epsilon_i < \epsilon_c \\ \epsilon_c & \text{if } n - \frac{1}{\beta} - \epsilon_i \geq \epsilon_c \end{cases} \qquad R_p = R_0 \exp \left[\frac{\sqrt{3}}{2} \epsilon_p - \frac{V_r}{2D} \right] \qquad (31)$$

If this expression yields $R_p < R_0$, then expansion is unstable from the onset and $R_p = R_0$ may be used instead.

D. Tabulated results for a few metals

This section tabulates shock and plastic work heating estimates for a few metals for the case of a cylinder driven by LX-14 to radial speed $V_r = 2702$ m/s. $D = 8800$ m/s, $\rho_x = 1835$ kg/m^3, and $\gamma_j = 2.947$ are used for LX-14 [22], based on parameter set 360A of the cited reference. E_x is taken to be 95% that of HMX [20] (LX-14 is HMX with 5% binder), giving $\sqrt{2E_x} = 2895$ m/s. P_1 is calculated by the method described in Section V-B. The assumed V_r corresponds to an Al6061-T6 cylinder with inner radius 3.175 cm and wall thickness 0.635 cm, based on Eq. 30. It is presumed that we adjust the wall thickness to give the same M and, therefore V_r, for the other metals tabulated.

Given $V_r/D = 0.307$, P_1 for the different metals, and the Steinberg parameters for the solid, the heating terms may be found. E_1 is calculated from Eq. 10. Bounds on E_s are calculated from Eq. 13. E_p is calculated from Eq. 19 at radius $R = 2R_0$ ($\epsilon = 0.978$ from Eq. 29) for the cases where E_s equals the lower and upper bounds due to shock heating (max and min here refer to E_s). The respective temperatures at each bound and stage are found from Eq. 12 for E_1 and from Eq. 14 for the other (zero pressure) terms. The expansion factor for onset of instability R_p/R_0 is found from Eq.31. $S_2 = S_3 = \epsilon_i = 0$ for the tabulated alloys. Silver is included since its high R_p/R_0 and unsurpassed electrical conductivity make it an intriguing, albeit expensive, option for an explosive generator armature.

	Al 6061-T6	Al 1100-0	Cu OFHC	SS 304	W	Ag
C_0 (m/s)	5240	5390	3940	4570	4030	3270
S_1	1.40	1.339	1.489	1.49	1.237	1.55
γ_0	1.97	1.97	2.02	1.93	1.67	2.4
b	0.48	0.48	0.47	0.50	0.38	0.56
Y_0 (MPa)	290	40	120	340	2200	50
Y_{max} (MPa)	680	480	640	2500	4000	660
β	125	400	36	43	24	28
n	0.10	0.27	0.45	0.35	0.19	0.8
$B/10^{-4}$ (K^{-1})	6.16	6.16	3.77	4.55	1.38	4.36
ρ_0 (kg/m^3)	2703	2707	8930	7900	19,300	10,490
C (J/kgK)	885	884	383	423	129	233
P_1 (GPa)	19.6	19.8	23.7	24.0	27.3	23.5
E_1, E_s max (kJ/kg)	578	575	155	158	51.0	148
E_s min (kJ/kg)	108	103	21.8	19.3	3.46	25.9
E_p min (kJ/kg)	136	52.1	44.6	109	159	82.1
E_p max (kJ/kg)	88	33.6	38.6	923	151	62.3
T_1 (K)	536	528	437	413	366	525
T_s min (K)	417	411	355	344	327	406
T_s max (K)	901	901	684	659	691	887
T_p min (K)	561	467	466	593	1535	549
T_p max (K)	987	935	777	864	1829	987
R_p/R_0	1	1.08	1.24	1.24	1	1.66

E. Comparison with CALE 2-D simulations

Results of a 2-D shock hydro simulations by program CALE [6] [7] are presented for comparison with the Al 6061-T6 and Cu analytic approximations, and to better quantify

E_s for which we have, at present, only broad bounds. We use 30 cm long liners with the same inner radius and mass as before and loaded with LX-14, for these simulations. The LX-14 is detonated at the left end of the cylinder on the z-axis ($r = z = 0$) at time $t = 0$. The simulations also assume the Steinberg model for the metal, so the test here is of the accuracy of our analytic approximations to the Steinberg model, as opposed to the model itself. Instead of the C-J EOS for the LX-14 products, though, CALE uses the Jones-Wilkins-Lee (JWL) EOS [30] with coefficients [22] A =11.65, B =0.5572, R_1 =5.4, R_2 =2.0, and ω =0.45. These parameters are taken from same consistent set of data (360A) as the C-J parameters used for the analytic model for maximum consistency. Note, though, that several alternative choices for LX-14 JWL coefficients are available in this reference and others [31] [32].

Figure 1 is a pressure map close-up of the Al 6061-T6 run 30 μs after detonation, when the detonation wave has reached $z \approx 26.4$ cm. One can see here the prompt detonation products (contour 9), the high pressure region behind the initial Al shock wave (contours 5 and 6), and the much lower pressure of the second shock transmitted outward through the Al (contour 1). Details are blurred due to the initial square mesh length of 0.714 mm. The peak pressure behind the Al shock is $P_1 \approx 20$ GPa, very similar to the value obtained by Neil's method.

Figure 2 shows the time history of total internal energy density of a fluid element in the Al 6061-T6 CALE simulation midway between the ID and the OD of the Al (to minimize edge effects due to the finite mesh size) and initially at z=16 cm (solid line). The element's radius increases by a factor of two at $t = 34.4$ μs, as labelled by the cross hairs on this curve. The results of the analytic model's upper and the lower bounds on $E_s + E_p$ are overlaid. Here, we assume E_s is instantaneously thermalizes upon shock transit and that thereafter the liner expands at the Gurney speed (Eq. 30) $V_r = 2702$ m/s in accord with Eq. 29, with only plastic heating occurring during expansion. The initial radius used for calculating plastic strain is that at mid wall. The difference between shock heating, as signified by the cross hairs at E_s min and E_s max, and the start of the energy ramp up is the initial plastic

work due to shear as the metal is assumed to jump suddenly to speed V_r. As with P_1, there is good agreement between the two models in regard to E_1 behind the initial Al shock (recall this equals E_s max, labelled by the upper left cross hairs). There is also reasonable agreement between the two models after shock dissipation ($t \approx 23$ μs) *provided* we assume $E_f \approx E_f$ min. The reason for this is clear from the small magnitude of the second shock ($t \approx 20$ μs). Apparently, the Al rarefaction wave efficiently couples to the explosive products, reflecting very little energy back outward as a second shock. $E_s \approx E_s$ min, then, may be assumed for HE driving Al. As the liner expands, though, the analytic model overestimates E_p vs. time. The reason for this is that plastic strain, and therefore heating, is primarily a function of expansion factor (Eq. 29), and the Gurney equation overestimates the average speed of the liner during the period shown. The expansion velocity at the doubled radius of the Al in the CALE run is only $V_r = 2500$ m/s, with 90% of this not attained until $t = 23$ μs (5 μs after shock arrival). The energy discrepancy is significantly less (analytic is 6 % higher) if one compares the models at the point were the radius at mid wall has doubled (right cross hairs).

Figure 3 shows the same plot as Fig. 2, but for the Cu cylinder. Here, the analytic model's lower bound results in an energy density at doubled radius 5% lower than for the CALE run. The analytic value there being lower this time may due to the (much denser) Cu having a greater impedance mismatch to LX-14 than Al, resulting in the second shock having a greater relative contribution. The Gurney speed overestimates V_r by about the same amount as it did for the Al run.

Acknowledgment

REFERENCES

[1] M. Lehr, G. Baca, D. Chama, K. Hackett, T. Hussey, J. Kiuttu, D. Shiffler, J. Graham, W. Sommars, D. Coffey, and T. Englert, in *Dig. of Tech. Papers, Eleventh IEEE International Pulsed Power Conference*, edited by G. Cooperstein and I. Vitkovitsky (IEEE, Cat. No. 97CH36127, 1997), pp. 579–584.

[2] J. B. Chase, D. Chato, G. Peterson, and P. Pincosy, in *Dig. of Tech. Papers, Eleventh IEEE International Pulsed Power Conference*, edited by G. Cooperstein and I. Vitkovitsky (IEEE, Cat. No. 97CH36127, 1997), pp. 1005–1009.

[3] D. J. Steinberg, Technical Report No. UCRL-MA-106439, change 1, Lawrence Livermore Nat'l Laboratory, FEB 1996 (unpublished).

[4] L. Knopoff, in *High Pressure Physics and Chemistry*, edited by R. S. Bradley (Academic Press, New York, 1963), pp. 227–245.

[5] D. J. Steinberg, S. G. Cochran, and M. W. Guinan, J. Appl. Phys. **51**, 1498 (1980).

[6] R. E. Tipton, in *Megagauss Technology and Pulsed Power Applications*, Fourth International Conference on Megagauss Magnetic Field Generation and Related Topics, edited by C. M. Fowler, R. S. Caird, and D. J. Erickson (Plenum Press, New York, NY, 1987), p. 299, also available as LLNL report UCRL-94277.

[7] R. E. Tipton, *CALE Users Manual* (Lawrence Livermore National Laboratory, MS L-35, P. O. BOX 808, Livermore, CA 94550, 1991).

[8] D. J. Cagliotro, D. A. Mandell, L. A. Schwalbe, T. F. Adams, and E. J. Chapyak, J. Impact Engrg. **10**, (1990).

[9] W. H. Lee, Comput. Methods Appl. Mech. Engrg. **156**, 149 (1998).

[10] D. J. Steinberg, Technical Report No. UCRL-93703, Rev. 1, Lawrence Livermore Nat'l Laboratory, Apr 87 (unpublished).

[11] R. E. Peterkin, Jr. and M. H. Frese, Technical Report No. MRC/ABQ-R-1191, Mission Reseach Corporation, 1720 Randolph Rd., SE, Albuquerque, NM 87106, Nov. 1989 (unpublished).

[12] J. M. Walsh, M. H. Rice, R. G. McQueen, and F. L. Yarger, Physical Review **108**, 196 (1957).

[13] W. E. Boyce and R. C. DiPrima, *Elementary Differential Equations*, 3rd ed. (John Wiley & Sons, New York, NY, 1997), p. 16.

[14] Y. B. Zel'dovich and Y. P. Raizer, *Physics of Shock Waves and High-Temperature Hydrodynamic Phenomena* (American Elsevier, New York, NY, 1966).

[15] H. Knoepfel, *Pulsed High Magnetic Fields* (American Elsevier, New York, NY, 1970).

[16] A. S. Kahn and S. Huang, *Continuum Theory of Plasticity* (John Wiley & Sons, Inc., New York, NY, 1995).

[17] R. W. Gurney, Technical Report No. report 405, Brooks Research Laboratory, 1943 (unpublished).

[18] N. E. Hoskin, W. S. Allan, W. A. Bailey, J. W. Lethaby, and I. C. Skidmore, in *Proc. Fourth Symposium (International) on Detonation* (Office of Naval Research, Washington, D. C., 1965), pp. 14–26, report ACR-126.

[19] O. E. Jones, in *Behavior and Utilization of Explosives in Engineering Design 12th Annual Symposium*, edited by L. Davison, J. E. Kennedy, and F. Coffey (ASME (NM Section), Albuquerque, NM, 1972).

[20] J. E. Kennedy, in *Behavior and Utilization of Explosives in Engineering Design 12th Annual Symposium*, edited by L. Davison, J. E. Kennedy, and F. Coffey (ASME (NM Section), Albuquerque, NM, 1972), pp. 109–124.

[21] E. L. Lee and H. Pfeifer, Technical Report No. UCRL-50545, Lawrence Livermore Nat'l

Laboratory, Jan 6, 1969 (unpublished).

[22] E. L. Lee, D. Breithaupt, C. McMillan, N. L. Parker, J. W. Kury, C. M. Tarver, W. Quirk, and J. Walton, in *Proc. Eighth Symposium (International) on Detonation, Albuquerque, NM* (Naval Surface Weapons Center, Silver Spring, Maryland, 1985), p. 613, report NSWC MP 86-194 (preprint available as LLNL report UCRL-91490, Rev. 1).

[23] J. W. Kury, H. C. Hornig, E. L. Lee, J. L. McDonnel, D. L. Ornellas, M. Finger, F. M. Strange, and M. L. Wilkens, in *Proc. Fourth Symposium (International) on Detonation* (Office of Naval Research, Washington, D. C., 1965), pp. 3–13, report ACR-126.

[24] T. Neal, in *Proc. Sixth Symposium (International) on Detonation* (Office of Naval Research, Arlington, VA, 1976), pp. 602–611, report ACR-221.

[25] A. H. Shapiro, *The Dynamics and Thermodynamics of Compressible Fluid Flow, Vol. I* (John Wiley & Sons, New York, NY, 1953).

[26] W. Fickett and W. C. Davis, *Detonation* (Univ. of CA Press, Los Angelas, CA, 1979).

[27] Y. B. Zel'dovich and A. S. Kompaneets, *Theory of Detonation* (Academic Press, New York, NY, 1960).

[28] G. E. Duvall and G. R. Fowles, in *High Pressure Physics and Chemistry, Vol. 2*, edited by R. S. Bradley (Academic Press, New York, 1963), pp. 209–291.

[29] J. Chakrabarty, *Theory of Plasticity* (McGraw-Hill, New York, NY, 1987), p. 6.

[30] E. L. Lee, H. C. Hornig, and J. W. Kury, Technical Report No. UCRL-50411, Lawrence Livermore Nat'l Laboratory, May 2, 1968 (unpublished).

[31] H. Hornberg, Propellants, Explosives, Pyrotechnics **11**, 23 (1986).

[32] R. E. Tipton, Eos Coefficients for the CALE Code for Some Materials, 1997, CALE documentation, unpublished.

Figure Captions

Fig. 1 Pressure map at 30 μs of a CALE simulation of a 3.81 cm OD, 0.635 cm thick, 30 cm long Al 6061 T-6 tube filled with LX-14 and detonated on axis at the left end.

Fig. 2 Internal energy density vs. time for Al 6061-T6 loaded with LX-14 midway between ID and OD of the cylinder, initially at z = 16 cm. CALE simulation (solid line). Upper and lower bounds from analytic model (dashed line). Cross hairs signify upper and lower bounds on dissipated shock heating (left) and the time on the respective curves where the radius has doubled (right).

Fig. 3 Same plot as Fig. 2, but for Cu (1/2 hard) loaded with LX-14.
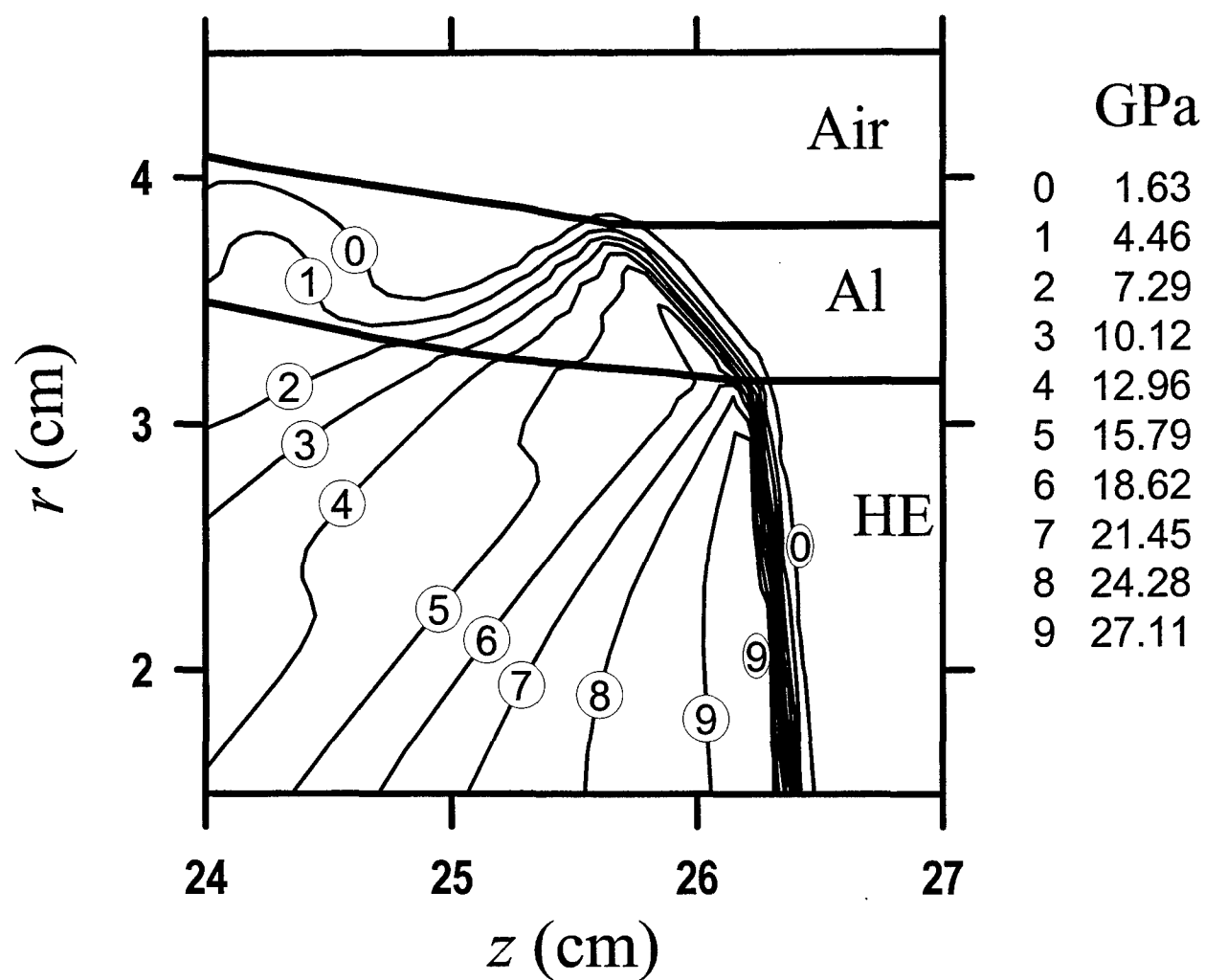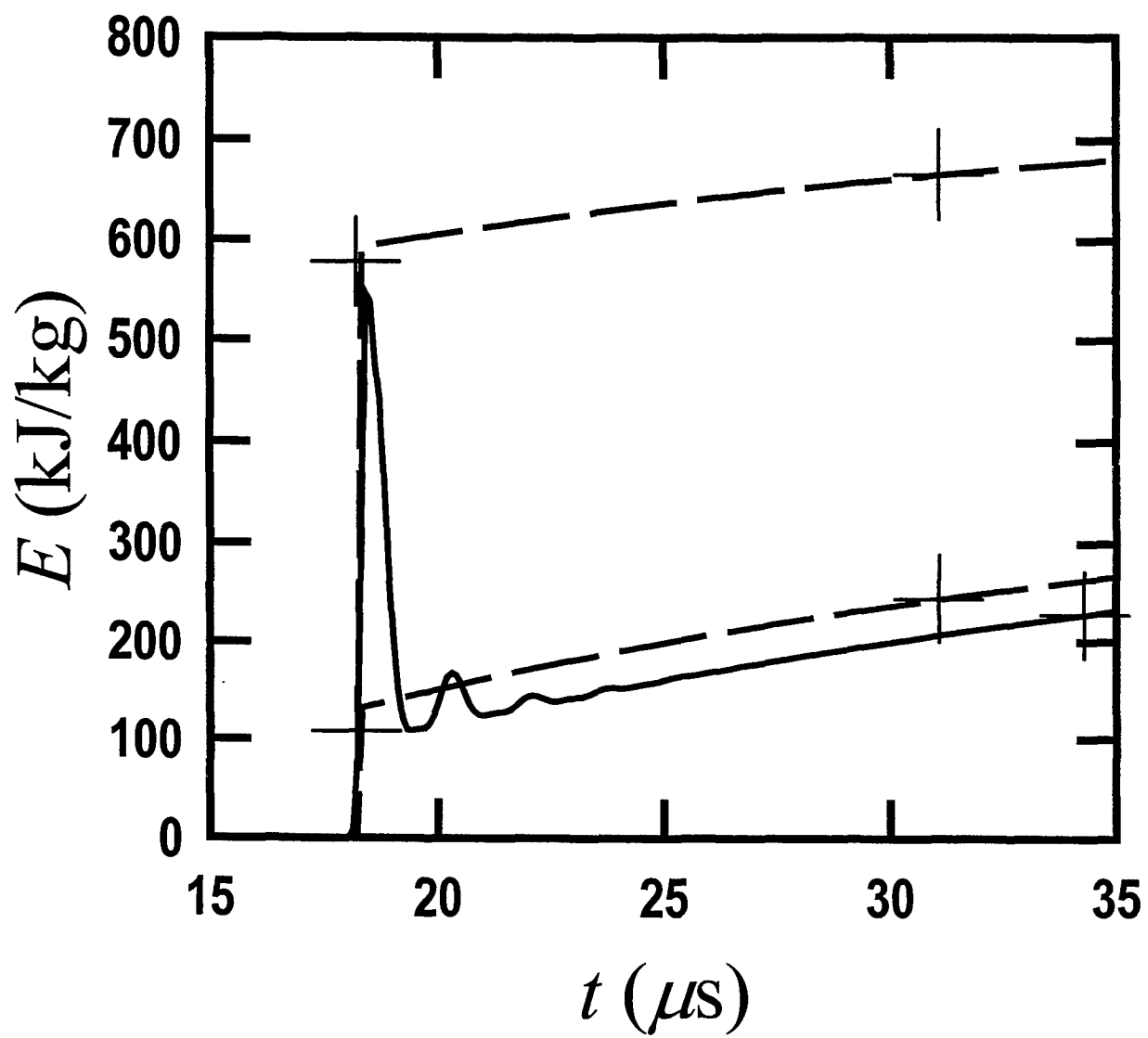
Fig. 1
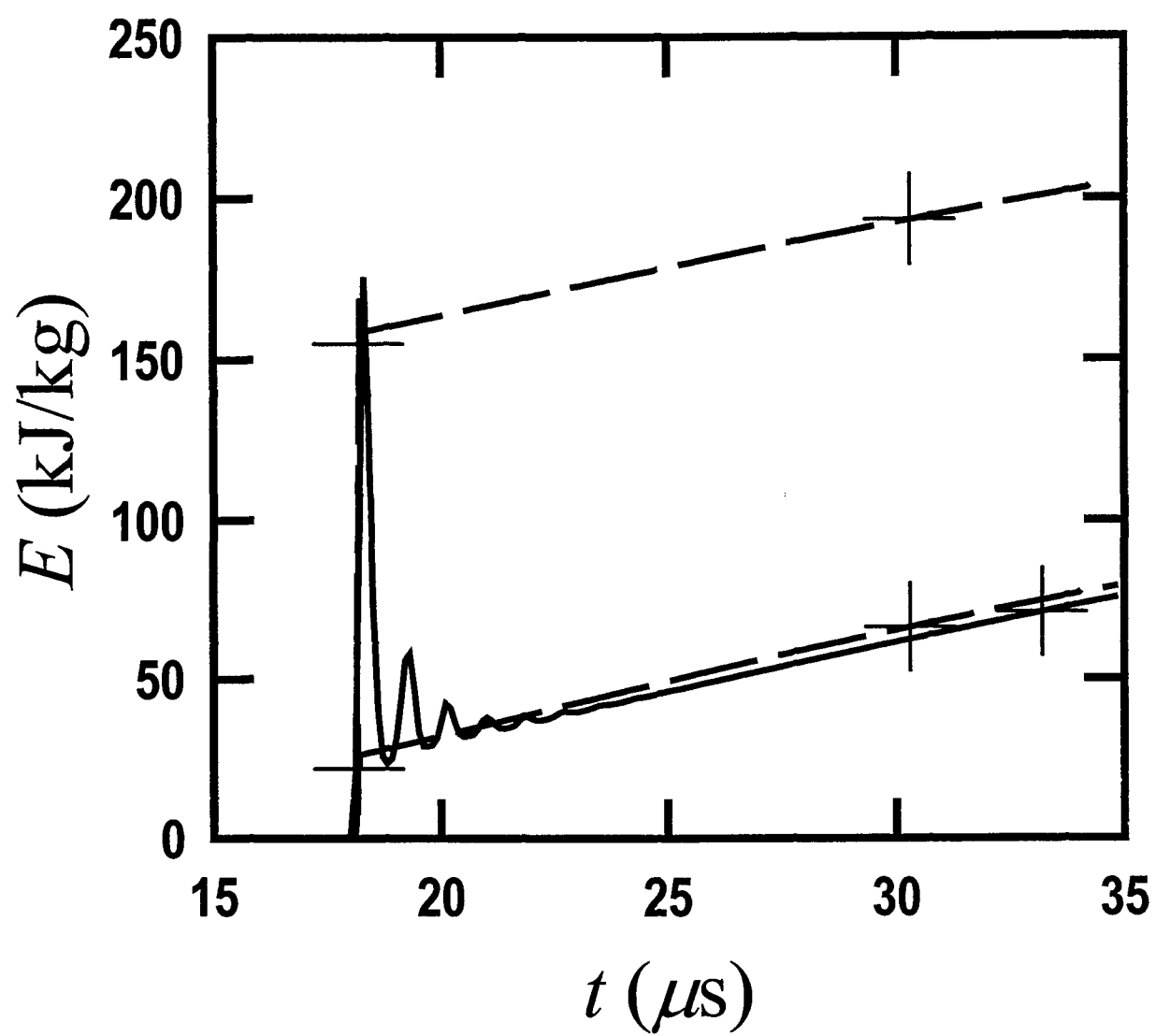
Fig. 2

Fig. 3

DISTRIBUTION LIST

DTIC/OCP
8725 John J. Kingman Rd, Suite 0944
Ft Belvoir, VA 22060-6218   1 cy

AFSAA/SAMI
1570 Air Force Pentagon
Washington, DC 20330-1570   1 cy

AFRL/VSIL
Kirtland AFB, NM 87117-5776   2 cys

AFRL/VSIH
Kirtland AFB, NM 87117-5776   1 cy

Official Record Copy
  AFRL/DEHP (Dr Ruden)   2 cy
  Kirtland AFB, NM 87117-5776